Window Impedance of Recorder-Like Instruments

Augustin Ernoult, Benoît Fabre

Window impedance of recorder-like instruments.

A. Ernoult[1)] [1], B. Fabre[1)]
[1)] Sorbonne Universités, UPMC Univ Paris 06, CNRS, UMR 7190, LAM, Institut Jean Le Rond ∂'Alembert, F-75005 Paris, France

Abstract

Sound production in recorder-like instruments occurs near an open end of the resonator. The impedance of this opening, specific to flute-like instruments, acts both on the passive resonances and on the active behaviour. The geometry of this active-end is characterized by the presence of an edge needed for the sound source. This edge induces a significant enlargement of the section of the chimney associated with this opening. This study proposes a model of the frequency response of the active-end of recorder-like instruments inspired by previous works on open side holes. Predictions from this model are compared with measurements of a hand made recorder and to finite element simulations. Multiple geometrical conditions are simulated via finite elements and compared with the proposed model.

1 Introduction

Flute-like instruments are musical instruments in which the sound source is created by a jet-edge interaction coupled with an acoustic resonator [1]. The jet is formed by applying supply pressure upstream from a channel, the outlet of which is directed towards the edge. The channel is formed either between the lips of the musician for transverse flutes, or by the instrument maker for recorders and organ pipes. All these instruments share a specific opening at the active end of the resonator where the sound source occurs. This opening between the outlet of the channel and the edge is called the window in this study. The jet-edge interaction induces a pressure difference Δp acting as a sound source.

The frequency of the sound generated by these instruments depends on the balance between the phase induced by the resonator and the delay associated with the convection of a perturbation along the jet[2, 3]. Due to the nature of the sound source, the frequency response of the resonator can therefore be characterized by the global admittance seen from the edge of the instrument Y_{tot}, which is a combination of the impedance of the pipe of the instrument Z_p and the impedance of the window Z_w [4] (Fig.1). Conservation of the acoustic flow between the pipe and the window gives[4, 1]:

$$Y_{tot}(\omega) = \frac{Q_{ac}(\omega)}{\Delta P(\omega)} = \frac{1}{Z_p + Z_w}, \tag{1}$$

[1] ernoult@lam.jussieu.fr

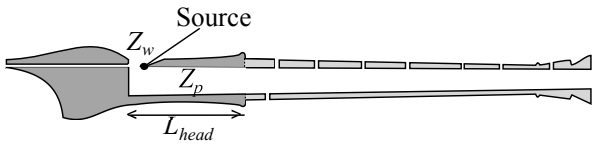

Figure 1: Cross sectional representation of a recorder with the two associated impedances Z_p and Z_w.

where Q_{ac} and ΔP are the Fourier transform of the acoustic volume flow rate and the pressure difference across the window. Most of the elements (bore, side holes, etc.) influencing the pipe impedance Z_p are common to woodwind instruments. A lot of studies have already been carried out on the influences of the different geometrical aspects on the pipe impedance. It is now possible to model it quite accurately. Most of the results have been summarized by Lefebvre [5]. Only a few studies have been led on the window impedance Z_w which is specific to flute-like instruments [4, 6, 7]. For all instruments with a fixed channel (recorder and organ pipe), the consequent fixed geometry follows the same global sketch, represented in Figure 2.

As seen from the acoustic flow, the duct which provides path connecting the inside to the outside is much complex. The acoustic flow changes direction through a right angle bend between the pipe of cross section S_p (rectangular for wooden organ pipes, and circular for the most of the other instruments) and the so-called window of cross section $S_w = WH$, where W is the distance between the outlet of the channel and the edge, and H is the width of the opening. This angle is followed by a short chimney of length l_e with a significant enlargement linked to the edge characterized by the angle α. The length l_e is most often due to the thickness of the wooden wall in which the edge is sculpted, but for the metallic organ pipe, the instrument makers may sometimes add little pieces of metal called *ears* surrounding the opening. The supply channel is not taken into account in this study. Its influence is perceptible only at specific frequencies. Furthermore, during playing, this influence is modified by the supply system which is also not taken into account here.

The instruments having a window imposed by the instrument maker will be called recorder-like instruments in this study. The geometry of a real window is more complex than the schematic representation of the figure 2b, in particular, the edge is not perfectly sharp. But in this study it is assumed that these 5 parameters (W, H, α, l_e, S_p) are the most important when considering the acoustic impedance at the window of a recorder-like instrument. This schematic representation is not directly applicable for metallic organ pipes. Indeed, with this schematic representation, the flat edge of these instruments would correspond to a null angle ($\alpha = 0$), which would induce infinitely long ears in the x direction. Results of this study must be used carefully for this type of instrument.

Flutes in which the jet is formed through the player's lips are out of the scope of the present study. Indeed, the window opening without the musician is very close to the classic

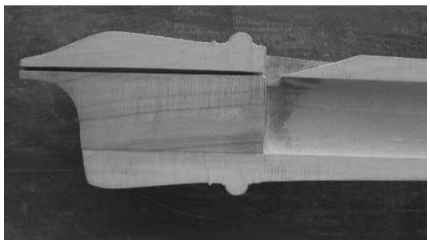

(a) *Photograph of a mouth-piece of recorder [8].*

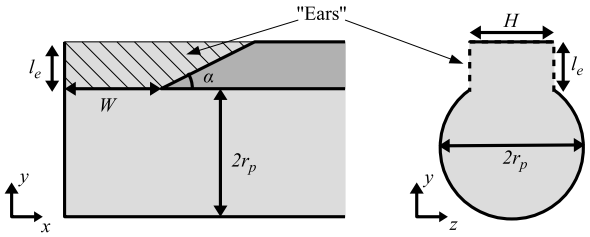

(b) *Sketch of a window.*

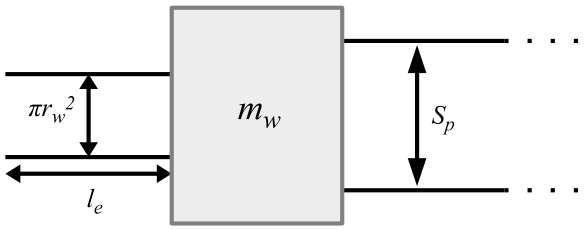

(c) *General model of a window.*

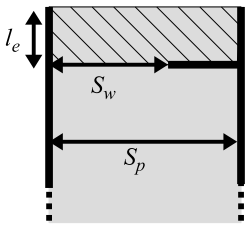

(d) *Rectangular geometrie associated with the model of Verge [15].*

Figure 2: Cross sectional representation of the window of a recorder: a photograph (a), the schematic representation (b), the general model associated (c), and the geometrie associated with the model of Verge [15] (eq.(11)*).*

open hole of a wood-wind instrument. The difficulty, in these instruments, is to take into account the influence of the musician on the radiation.

The paper is structured as follows. In the first part, the window impedance is measured for a restricted number of geometries. Due to the number of independent geometrical parameters, an experimental study of the influence of each parameter on the window frequency response would require a very large set of geometries. In the second part, finite element calculations are therefore used to simulate a large number of window geometries, which allows predicting the variation of the impedance with the different geometric parameters. These numerical results are then used to build a model inspired from the models used for the open side holes. Finally the results and the assumptions used in the model are discussed.

2 Measurement of window impedances

The window impedance can't be measured directly because the window of a recorder can't be dissociated from the instrument. It is possible to estimate it at low frequencies from the measurement of the impedance of the head of the instrument. The head of a recorder is the part with the window and the mouth piece and without tone-holes (in dark grey in Fig.1). The head can be dissociated from the body of most recorders. An impedance sensor [9] is placed at the outlet of the head to measure the impedance Z_{head}. The tube between the outlet of the head and the edge of the recorder is assumed to be cylindrical, with a radius r_p (cross-section S_p) and a length L_{head} (Fig.1, 2). For each instruments measured, the pipe diameter shows a variation about $0.1mm$ according to the axes of the pipe or the orientation. Under the assumption of plane waves ($kr_p \ll 1.8$), the window impedance Z_w can be obtained from the head impedance Z_{head} using the transfer matrix of a cylinder given by the formula [5, 10]:

$$Z_w(\omega) = \frac{Z_c \tanh(\Gamma L_{head}) - Z_{head}(\omega)}{\frac{Z_{head}(\omega)}{Z_c} \tanh(\Gamma L_{head}) - 1}, \tag{2}$$

where Γ is the complex propagation coefficient and Z_c is the characteristic impedance of the cylinder. These two parameters (Γ and Z_c) are dependent on the tube cross-section S_p and they take into account the visco-thermal losses through the following expressions [11]:

$$\left\{ \begin{array}{rcl} \Gamma & = & jk\phi_\Gamma \quad , \\ Z_c & = & \frac{\rho c}{S_p}\phi_{Z_c} \quad , \end{array} \right. \tag{3}$$

where ρ is the density of the air, c is the speed of sound, and ϕ_Γ and ϕ_{Z_c} are two dimensionless functions [11] introducing corrections due to viscous and thermal effects on the propagation. The two dimensionless functions are function of the Stokes number similar to a dimensionless radius: $r_v = r_p\sqrt{\omega\rho/\eta}$, where η is the shear viscosity coefficient. The values of the density ρ, the speed of sound c and the shear viscosity η are estimated knowing the temperature[11]. For high values of the Stokes number, a second order series expansion in $1/r_v$ gives [10]:

$$\left\{ \begin{array}{rcl} \phi_\Gamma & = & 1 + \frac{\alpha_1\sqrt{-2j}}{r_v} - j\frac{\alpha_2}{r_v^2} \\ \phi_{Z_c} & = & 1 + \frac{\beta_1}{r_v} + \frac{\beta_2}{r_v^2} \quad , \end{array} \right. \tag{4}$$

where $\alpha_1, \alpha_2, \beta_1, \beta_2$ are coefficients depending on the Prandtl number P_r and of the heat capacity ratio γ. For the air, these two coefficient are assumed to be constant ($P_r = 0.71$ and $\gamma = 1.402$) which gives: $\alpha_1 = 1.044$; $\alpha_2 = 1.080$; $\beta_1 = 0.370$ and $\beta_2 = 1.147$ [10].

This protocol is used to measure the window impedances of five Aesthe hand-made recorders already used by Blanc [12]. The geometrical parameters of their windows are indicated in table 1. The frequency domain explored is $100Hz < f < 5kHz$. The window impedance measured on the alto recorder is plotted in Figure 3.

	Bass	Tenor	Alto	Sop.	Sop.^{ino}
α (°)	17	17	15	15	13
l_e (mm)	7.5	6.5	5.6	4.0	2.6
r_p (mm)	16.0	11.2	8.8	6.6	5.3
H (mm)	19.2	14.5	12.2	9.5	7.50
W (mm)	7.5	4.5	4.45	3.0	3.0

Table 1: Geometric parameters of the windows of five hand-made recorders. Note that W represents the acoustical opening and does not include the chamfers as opposed to Blanc [12], where W represent the jet length including the chamfers.

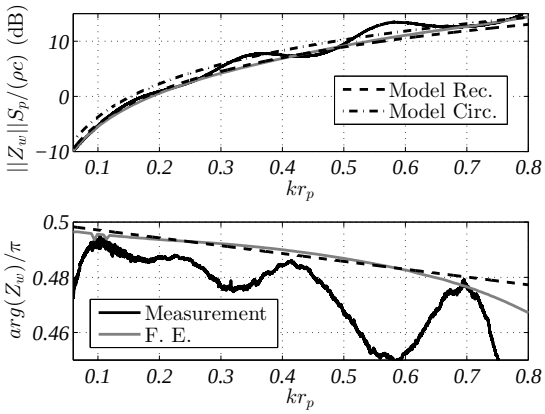

(a) Module and phase of impedance.

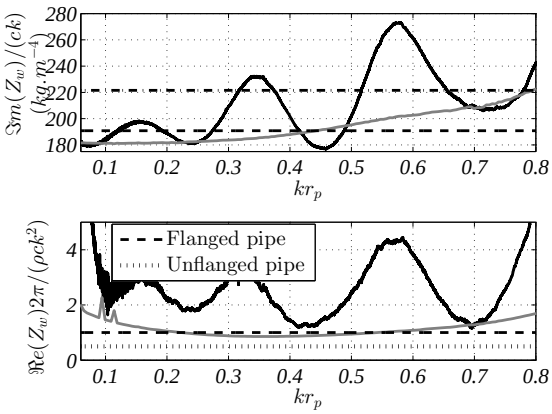

(b) Imaginary part normalyzed by kc to have inertance dimension, and real part normalized by $\rho ck^2/(2\pi)$.

Figure 3: Impedance of the tenor recorder from the measurement (solid black line), the finite element simulation (gray line) and the model of the window impedance Z_w . Modelled impedances use inertance of rectangulare (dashed line, Eq.(16)) or cylindrical (dashed-dotted line, Eq.(17)) rigth angled duct. The effect of using flanged or unflanged pipe (dotted line) is only plotted on the real part where the effect is particularly visible. The wave number k is normalized by the inner radius r_p of the head of the instrument.

The supply channels, not taken into account in this study, are blocked in the measurements presented here to avoid the resonance at $\lambda = l_c/2$, where l_c is the length of the channel. The window impedance of the tenor recorder estimated with this protocol is presented in Figure 3. Some oscillations appear in the measurements both in phase and amplitude (or real and imaginary parts) (Fig.3). This irregularities are also present with other recorders. In the protocol used here, the window impedance Z_w is only a small correction of the input

impedance of the head Z_{head}. All imprecisions in measurements or in the model used for the head pipe have large influences on the estimated window impedances. These irregularities could therefore be related to measurement issues as a poor signal-to-noise ratio at the anti-resonances of the head input impedance. But they may also be attributed to the model used for the head: a poor evaluation of the visco-thermal losses, or inaccuracies in the geometrical description such as in the length measurement due to irregularities on the plate surface under the window (on the left in Fig. 2b).

In spite of these irregularities, the imaginary part seems to be more or less proportional to the pulsation ($\omega = kc$) in low frequencies ($kr_p < 0.5$) (Fig.3b). The standard deviation related to the oscillations is around 20% for all recorders measured [2] but no global evolution with the wave number appears on the normalized imaginary part (Fig.3b). Numerical simulations are therefore used to confirm this observation while avoiding the experimental problems evoked.

3 Finite element simulations.

A large set of instruments should be studied to observe the influence of each of the five geometric parameters described in the introduction. In view of of the difficulty and the time necessary to make this number of instruments added to the experimental issues encountered, the acoustic flow in the geometry of the window is simulated using finite elements, providing results for a large number of different geometries.

The geometry of the windows simulated with finite elements is based on the sketch of the figure 2b. The mesh used is a 3D adaptation of the 2D mesh used by Auvray [14](Fig. 4). It includes a tube of cross-section S_p and length L_p, a radiation domain, and the window. The window is characterised by its width W, its depth H, the angle α of the triangular edge and the height l_e of the ears (Fig.2b). The generation of a 3D mesh which is not a simple transformation of a 2D mesh shows some difficulty. The target of the study is not the propagation of the waves into the tube. To simplify the generation of the mesh, the tube of the resonator is therefore taken rectangular with a height h_p and a depth H. To compare simulations and measurements of recorders, the dimensions of the tube are chosen with the same cross-sectional area as the cylindrical recorder head ($S_p = \pi r_p^2 = h_p H$). For a given geometry and assuming a frictionless adiabatic flow, the Helmholtz equation (Eq.(5)) is solved, with the FreeFEM++ solver [13], for different values of the wave-number k:

$$\Delta P_{ac}(\omega) + k^2 P_{ac}(\omega) = 0. \tag{5}$$

$P_{ac}(\omega)$ is the amplitude of the acoustic pressure for a given pulsation. A homogeneous pressure $P_{ac} = p_{ac}^0$ is imposed on the cross-section at the extremity of the tube. Rigid boundary conditions are imposed on the wall, i.e. a zero normal acoustic velocity: $\frac{\partial P_{ac}}{\partial n} = 0$,

[2] The mean values and standard deviations are presented in Figure 10

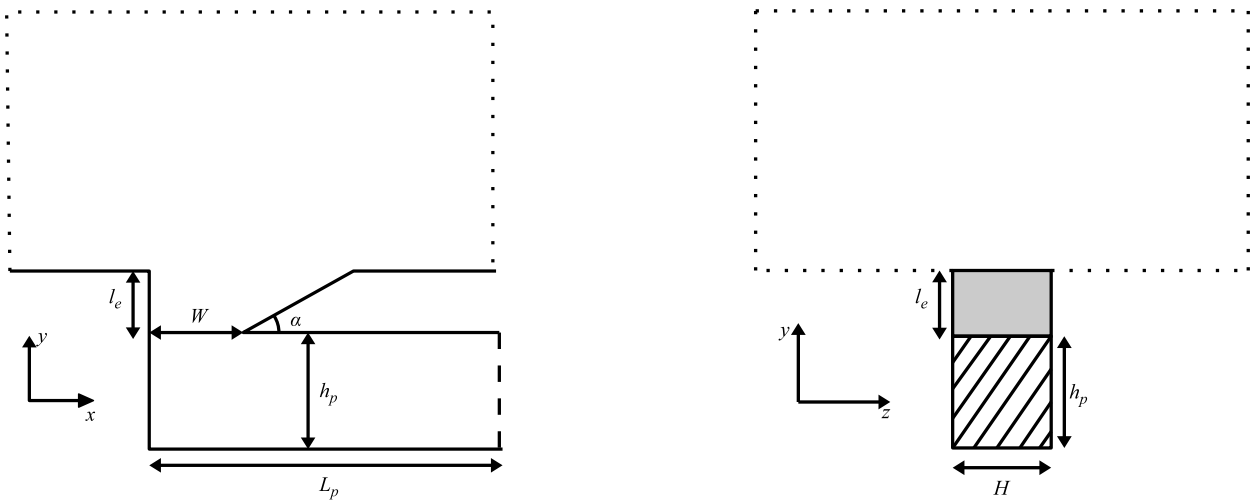

(a) *xy plane.* (b) *yz plane.*

Figure 4: Schematic representation of the computational domain. Rigid boundary conditions (zero normal velocity) are imposed on continuous lines and grey surfaces. The dashed lines and the hatched surfaces correspond to the entry of the rectangular tube where a homogeneous pressure is imposed. On dotted lines, a perfectly matched layer condition is imposed.

where n is the normal direction of the wall. To limit the influence of the boundary of the calculated radiation domain, artificial damping is added at the limit of the radiation domain which respects the perfectly matched layer condition ($\frac{\partial P_{ac}}{\partial n} = -ik(1+i\epsilon)P_{ac}$, with $\epsilon = 1$ controlling the damping). Only an upward radiation domain is considered. It excludes any possible diffraction by the body of the recorder which is supposed to be negligible.

The tube and the radiation domain are long enough to assume that the boundary conditions do not influence the response of the window. The tube is taken to be long enough to ensure a plane wave at its extremity ($L_p = 0.3\lambda$ with λ the wave length), which is coherent with the boundary condition imposed. The mesh has to be fine enough to correctly describe the window. These two conditions restrict the frequency domain which can be studied with a reasonable number of elements. The lowest frequency is fixed to $f > 100Hz$ which is the same as the one used for the measurements. The highest frequency is selected to match the cut-off frequency of the tube: $f < (\frac{2c}{h_p}, \frac{2c}{H})$.

As for the measurements, the window impedance can't be obtained directly from the simulation, but has to be evaluated from the input impedance at the end of the tube. This input impedance is calculated from the pressure field which results from solving the

Helmholtz equation (5):

$$Z_{input} = \frac{p_{ac}^0 S_0}{\int\limits_{S_0} \mathbf{V_{ac}} \mathbf{dS}} = ik\rho c \frac{p_{ac}^0 S_0}{\int\limits_{S_0} \frac{dP_{ac}}{dx} dS}, \tag{6}$$

where S_0 is the cross-section area of the end of the tube, and the acoustic velocity $\mathbf{V_{ac}}$ is obtained from the spatial derivative of the acoustic pressure P_{ac}. To obtain the window impedance from this input impedance, a formula similar to Eq.(2) is used, by replacing Z_{head} and L_{head} by Z_{input} and L_p. Following the frictionless and adiabatic hypotheses, the visco-thermal losses are not taken into account in the simulation, so $\Gamma = ik$ and $Z_c = \rho c / S_p$ ($\phi_\Gamma = \phi_{Z_c} = 1$). The window impedance Z_w is finally written as:

$$Z_w(\omega) = \frac{Z_c \tanh(ikL_p) - Z_{input}(\omega)}{\frac{Z_{input}(\omega)}{Z_c} \tanh(ikL_p) - 1}, \tag{7}$$

The assumption used for the boundary condition and the method to obtain the window impedance are first tested on a well-documented simple geometry: an open cylinder. After validation, this method is applied to the geometries of the recorders. About 430 sets of geometrical parameters are simulated. The window impedance obtained for the alto recorder is compared with the measured one presented in Figure 3. Certainly due to the approximations used in the finite element simulations (rectangular tube, limited radiation domain, walls without thickness, etc.), the amplitude simulated is globally slightly lower than the measured one. Furthermore, the small irregularities in the measurements already discussed (sec.2) are not present in the finite element simulation. Due to these differences, the standard deviation of the amplitude at low frequencies ($kr_p < 0.5$ and $kl_e < 0.5$) between finite element simulations and measurements is around 10% (bass:14%, tenor: 9%, alto: 10%, soprano: 8%, sopranino: 14%). The experimental irregularities are very small for the phase (only 0.02π radians of magnitude). The phases measured and simulated are therefore very closed. At low frequencies the standard deviation stays under 5% (bass:1%, tenor: 1%, alto: 5%, soprano: 3%, sopranino: 2%).

The absence of these irregularities allows to have a better understanding of the evolution of the window impedance with the frequency. In particular, the imaginary part normalized by the pulsation ($\omega = kc$) seems correctly approach by a constant in low frequency ($kr_p < 0.5$) (Fig. 3b). These observations seem indicate that the finite elements simulations are a good alternative to measurements to develop a predictive model of the window impedance.

4 Predictive Model

In most studies [2], the window impedance is described as a simple radiation impedance of a flanged pipe, similar to a length correction $l_r = 0.8216 r_w$, where r_w is the radius

of the opening. This radius is sometimes taken as the equivalent radius of the window $\sqrt{S_w/\pi}$ [2, 10], or sometimes as that of the resonator: r_p [15]. In some studies the length of the *ears* l_e is added [15].Finally the sharp edge is modeled by Verge [15] as a slit of cross-sectional area S_w into a pipe of cross-sectional area S_p which adds an inertance to the impedance. The inertance, or "acoustic mass", has dimensions of mass over a squared surface area. All these descriptions can be summarized in one global model inspired by the model traditionally used for the impedance of tone-holes [16, 17, 5]. The window is modelled as a short radiating cylindrical tube of length l_w and radius r_w in which the visco-thermal losses are neglected, and an inertance m_w (Fig.2c). The global expression of the window impedance is:

$$Z_w(\omega) = Z_{cyl}(l_w, r_w) + j\omega m_w, \tag{8}$$

where the input impedance $Z_{cyl}(l_w, r_w)$ of an open flanged pipe of length l_w and radius r_w equals:

$$Z_{cyl}(l_w, r_w) = \frac{\rho c}{\pi r_w^2} \tan\left(jk(l_w + l_r) + \frac{\beta}{2}(kr_w)^2\right), \tag{9}$$

where β is a coefficient dependent on the dimension of the space in which the radiation occurs. If the visco-thermal losses as neglected in the window, this coefficient is a constant. The two reference cases are the infinite space (unflanged pipe) for which $\beta = 0.5$ and the semi-infinite space (flanged pipe) for which $\beta = 1$ [18, 10]. Under the low frequency approximation, when the wave length is longer than the other dimensions ($\lambda \gg (l_w, r_w, r_p)$), the impedance can be simplified as:

$$Z_w(\omega) = j\omega M_w + \beta\frac{\rho c}{2\pi}k^2. \tag{10}$$

The length l_w and l_r are included in a global inertance $M_w = m_w + \frac{\rho}{\pi r_w^2}(l_w + l_r)$. In this formulation, only the imaginary part of the impedance is a function of the geometry through the global inertance M_w. The dimension of the space in which the radiation occurs is not obvious. The real parts of the measured, simulated and calculated impedances are compared in Figure 3b. The unflanged pipe formula gives values which are too small whereas the flanged pipe formula fits the simulated data well for $kr_p < 0.5$. The real part of the measurement is particularly sensitive to the irregularities. The minima of the real part correspond to the theoretical values in the case of a flanged pipe. This theoretical value is finally chosen for the real part of the impedance: $\beta = 1$. The real part of the impedance simulated by finite elements appears to be very similar to the one measured and predicted for an open side hole by Dalmont et al. [17].

The most precise model of the inertance M_w is the one proposed by Verge [15] for rectangular organ pipes, associating the presence of the edge to a slit of cross-section $S_w = WH$ into a rectangular pipe of cross-section S_p (Fig. 2d). Following Morse and Ingard [19], the corresponding inertance is written as:

$$\begin{cases} M_{Verge} &= m_{slit} + \frac{\rho}{S_p}\left(l_e + 0,82r_p\right). \\ m_{slit} &= \frac{4\rho}{\pi H}\ln\left(\frac{1}{2}\tan\frac{\pi W}{4H} + \frac{1}{2}\cot\frac{\pi W}{4H}\right) \end{cases} \tag{11}$$

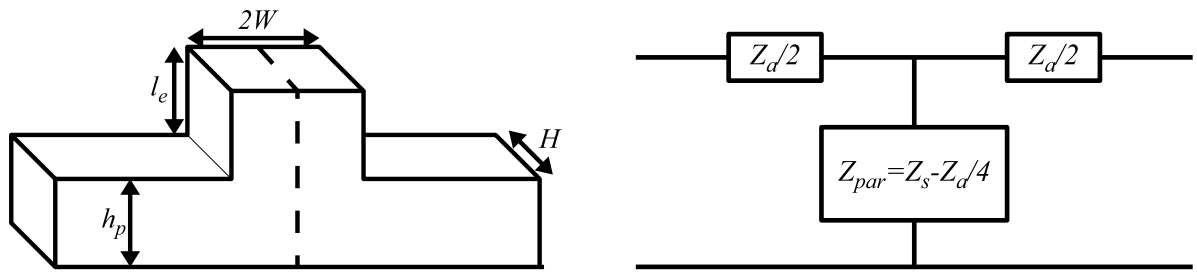

(a) Sketch of a side hole. (b) Block diagram of a side hole.

Figure 5: Sketch of a rectangular tube with a side-hole and equivalent block diagram

This model has been validated on around 10 geometries with only different ratio W/H. This formulation is associated with a strong simplification of the geometry (Fig. 2d) which could be valid only for specific cases. The edge being modelled by a slit, it is equivalent to an edge with a null angle ($\alpha = 0$), and only geometries with a sharp edge can be well modelled. Furthermore, in this model, the pipe diameter is the same on both sides of the edge. This assumption on the "effective" radius of the chimney has no geometrical support. This choice influences the radiation length correction $(0,82r_p)$ and the inertance of the ears $(\rho l_e/S_p)$ besides the slit's inertance. The purpose of this study, is therefore to propose a model without these limitations and validated on much more geometries.

For both measurements and finite element simulations, the value of the global inertance can be easily estimated with a simple linear regression on the imaginary part of the window impedance. The frequency domain used for this estimation is restrained to $100Hz < f < (c/(2r_p), c/(2l_e))$ to guarantee the low frequency approximation. The inertance depends on all the geometric parameters of the window. When the angle $\alpha = \pi/2$, the window is similar to the classical right angled duct, which is a geometry well described in the literature.

4.1 Duct with right angle

For $\alpha = \frac{\pi}{2}$, the geometry used in the finite element simulations is a right angle bend with rectangular cross-section. The study of a right angle bend is similar, in some aspects, to that of a side hole with a chimney, or to that of a T-joint (Fig.5a). Dubos [16] proposes to model the impedance of such a tone-hole by two impedances: one impedance linked to the symmetric modes Z_s and one impedance linked to the antisymmetric modes Z_a (Fig.5b). They are related to the inertances m_s and m_a. The impedance of the chimney, which is generally described as an open radiating cylinder of length l_{chim} and radius r_{chim}, is added

to the impedance of symmetric modes, which gives:

$$Z_a = j\omega m_a \quad (12)$$

$$Z_s = j\omega m_s + Z_{cyl}(l_{chim}, r_{chim}) \quad (13)$$

with Z_{cyl} from Eq.(9). The works of Morse and Ingard [19] and Thompson [20] corrected by Bruggeman [21], show that the impedance of a right angle bend has the same form as the impedance Z_s. Electrical analogy and analytical calculus show that the inertance of the right angle impedance is the twice the inertance of the side hole plus the equivalent mass of the bend volume [22, 16, 10]. In these studies this volume is already taken into account in the length of the main tube (Eq.(2) and (7)). Finally, the inertance associated with the right angle bend is simply $m_{ra} = 2m_s$. In the geometry of the window, when $\alpha = \pi/2$, the "chimney" has the length of the ears $l_{chim} = l_e$ and an equivalent radius $r_{chim} = r_w = \sqrt{WH/\pi}$, which gives, in the low frequency approximation:

$$Z_w(\alpha = \frac{\pi}{2}) = j\omega \left(m_{ra} + \frac{\rho}{S_w}(l_e + l_r) \right) \quad (14)$$

$$M_w(\alpha = \frac{\pi}{2}) = m_{ra} + \frac{\rho}{S_w}(l_e + l_r) \quad (15)$$

The relation between the inertance and the length of the ears can be easily verified by varying this length l_e keeping all the other geometric parameters constant in finite element simulations (Fig. 6). The zero coordinate of the linear regression summarized the inertance of the right angle and the radiation length correction.

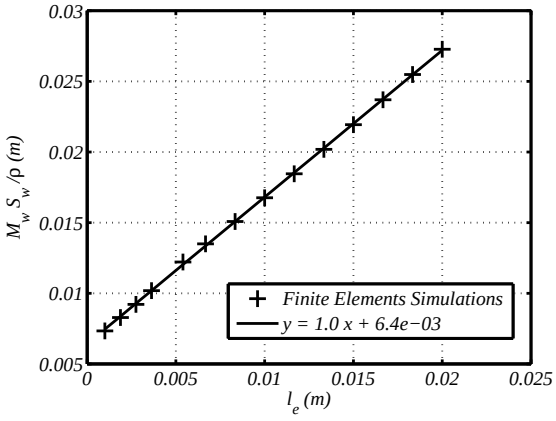

Figure 6: Relation between the inertance M_w and length of ears l_e for fixed cross-sections($W = 4.5mm$, $H = 12.2mm$ et $S_p = 2.4cm^2$).

Lebfevre [5] summarized the different studies on tone-hole impedance. For rectangular tubes, an analytical formulation obtained by conformal mapping exists[16, 22, 20]. For the

right angle of this study, it gives:

$$m_{ra}^{(rec.)} = \frac{2\rho}{\pi H}\left[\ln\left(\frac{1+\delta^2/4}{2\delta}\right) + \frac{2}{\delta}\left(1-\frac{\delta^2}{4}\right)\arctan\left(\frac{\delta}{2}\right)\right], \tag{16}$$

with $\delta = \frac{2W}{h_p} = \frac{2WH}{S_p}$ (Fig.5a). For circular tubes, several numerical estimations exist [23, 24, 16]. With the geometry studied here, the formulae proposed by Keefe[24] and Dubos[16] give similar results. For the geometry of this study, the formula of Dubos gives for example:

$$m_{ra}^{(circ.)} = \frac{2\rho}{\pi r_w}\left(0.82 - 0.193\zeta - 1.09\zeta^2 + 1.27\zeta^3 - 0.71\zeta^4\right), \tag{17}$$

with $\zeta = \frac{r_w}{r_p}$.

The effect of the length correction l_r and its relation to the radius is not straight forward. Indeed, the modifying the cross-sectional area S_w also modifies the inertance of the right angle. The radius is assumed to be the equivalent radius of the cross-section.An a posteriori optimization gives $l_r = 0.695 r_w$. This value is coherent with the results obtained by Dalmont [25], from which the length correction of a lateral hole should be between the length correction of a flanged pipe ($l_r = 0.816 r_w$) and the one of an unflanged pipe ($l_r = 0.613 r_w$). Finally, for a fixed geometry of the right angle bend, the inertance associated with the corner can be evaluated by subtracting the inertance $(\rho l_r)/S_p$ to the intercept of the linear regression of the variation of M_w with l_e. The values obtained for different geometries, with different W, H or height of the main tube, are compared with the values obtained from the two formulae (Fig. 7). For comparison purposes, the equivalent radii for the circular tube are taken: $r_i = \sqrt{S_i/\pi}$, with $i = w, p$.

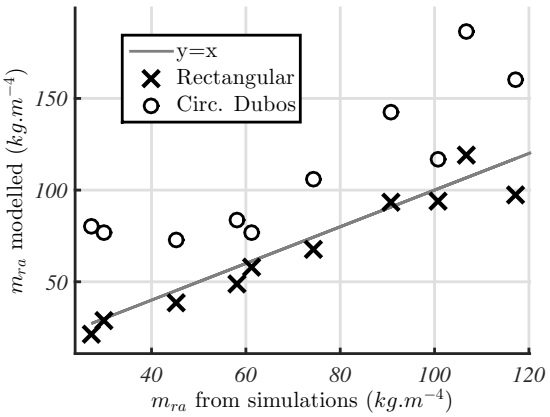

Figure 7: Inertance associated m_{ra} with the right angle predict by the formulae of the equations (16) *and* (17) *compared with the values obtained from the finite element simulations.*

As expected, the formula for the inertance of a right angle bend with rectangular cross-sections fits well the data obtained from the finite element simulations. In the case of a real recorder, the cross-section of the main tube is circular and the cross-section of the ears is rectangular. The choice between the two hypotheses is not obvious. For the finite elements, the expression for the inertance of a rectangular right angle bend is used in the remainder of the study.

4.2 Influence of the angle α

When the angle $\alpha < \pi/2$, the right angle of the duct is follow by an enlargement due to the sharp edge (Fig.2). Assuming that the inertance linked to the right angle bend does not change with the value of α, it is verified that the effect of the angle is not influenced by the cross-sectional area of the main pipe S_p. The total inertance can then be written as:

$$\left\{ \begin{array}{lcl} M_w & = & m_{ra} + m_\alpha + \frac{\rho}{WH} l_r, \\ m_\alpha(\alpha = \pi/2) & = & \frac{\rho l_e}{WH}, \\ l_r(\alpha = \pi/2) & = & 0.695\sqrt{WH/\pi}, \end{array} \right. \tag{18}$$

with m_{ra} given by the equations (16) or (17).The influence of the angle α can be decomposed into an inertance linked to the enlargement of the cross-section due to the presence of the edge m_α and into a length correction linked to the radiation l_r. The influence of the edge is modelled in this study by the inertance associated with the mass of fluid above the edge. Based on the works of Lyons [6] and Steebergen [7], this inertance can be calculated as follows:

$$m_\alpha = \rho \int_{y=0}^{y=l_e} \frac{dy}{S(y)} \tag{19}$$

$$= \frac{\rho}{H} \int_{y=0}^{y=l_e} \frac{dy}{W + \frac{y}{\tan(\alpha)}} \tag{20}$$

$$= \frac{\rho}{H} \tan(\alpha) \ln \left[1 + \frac{l_e}{W \tan(\alpha)} \right] \tag{21}$$

where $S(y)$ is the cross-sectional area of the pipe above the edge ($S(y=0) = WH$). To obtain the values of m_α, from the inertance M_w estimated on simulations and the equation (18), it is necessary to know the length correction l_r. An assumption about the length correction of radiation has to be made to estimate the inertance due to the angle. In a first approximation, this length correction is assumed independent of the angle α: $l_r(\alpha, W, H) \approx 0.695\sqrt{WH/\pi}$. This hypothesis can be verified a posteriori. The values of m_α estimated from the simulations with Eq.(18) and this hypothesis are compared with the model in Figure 8.

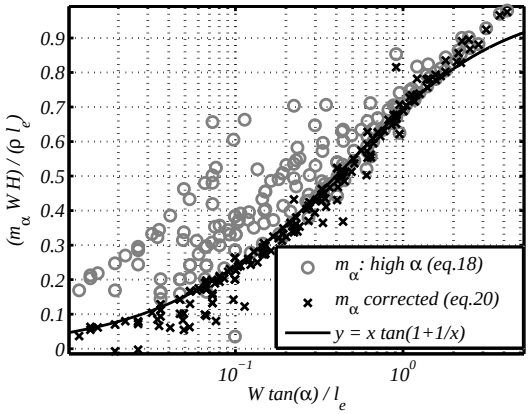

Figure 8: Values of m_α estimated from finite element simulations with Eq.(18)*, normalized by $\frac{\rho l_e}{WH}$ as a function of the dimensionless variable $\frac{W\tan(\alpha)}{l_e}$. They are compared with the analytical formula of equation* (21)*.*

The formulation of Eq.(21) fits well the data from the geometries with high values of the angle α, but not for the lowest values. Indeed, the equation (21) suggests that the value of the inertance m_α approaches zero when the angle approaches zero. This effect is not verified by the finite element simulations (Fig.8). Furthermore, this formula suggests that adding *ears* on a flat edge ($\alpha = 0$) should have no effect on the radiation. In a slightly different way, this action is made by the organ makers on metallic pipes.

The mesh used for the finite element simulations cannot simulate a null angle, which implies the superposition of two surfaces. But it is possible to observe the evolution of the inertance as a function of the geometry of the window for the lowest value of angle simulated ($\alpha = 0.09$ rad) (Fig.9). It appears that $m_\alpha(\alpha \approx 0)$ is independent of the width W, of the window. Its value approaches zero when the ears are short, and evolves as the square root of the ratio l_e/H. A fit of the data gives

$$m_\alpha(\alpha \approx 0) = 0.85\frac{\rho}{H}\sqrt{\frac{l_e}{H}} \tag{22}$$

Two asymptotic behaviors are finally identified. The inertance is well estimated by the equation (21) for the highest value of α and it is estimated by the equation (22) for $\alpha = 0$. These two behaviors can be seen as two different descriptions of the flow above the edge. For high values of α, the flow is constrained in three dimensions, whereas for very low values of α, the flow is only constrained under two dimensions (y, z in Fig.2b and Fig.4). The link between these two behaviors is chosen by adding the estimation of equation (22) weighted by a factor $C^{-\alpha}$ to the model of Eq.(21). The value of the coefficient C is optimized to fit the data.

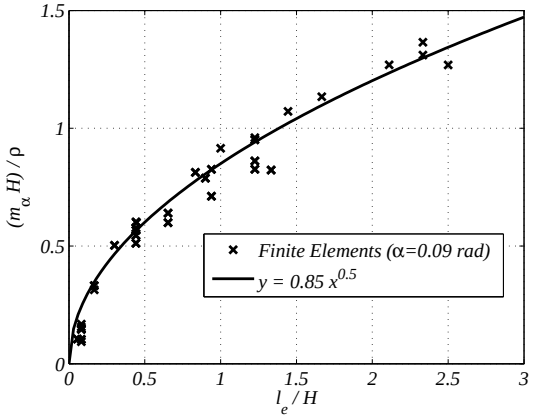

Figure 9: Values of m_α for $\alpha = 0.09rad$ estimated from finite element simulations with Eq.(18)*, normalized by $\frac{\rho}{H}$ as a function of the ratio $\frac{l_e}{H}$. They are compared with the analytical formula of equation* (22)*.*

$$m_\alpha = \frac{\rho}{H}\tan(\alpha)\ln\left[1+\frac{l_e}{W\tan(\alpha)}\right] + 32^{-\alpha}\frac{\rho}{H}0.85\sqrt{\frac{l_e}{H}} \tag{23}$$

It is now possible to give a global formulation of the window inertance, and also the window impedance, by combining the equations (8),(18),(23) and (16). The inertances calculated with this model are compared with the value of the inertances estimated from finite element simulations for the 444 different geometries simulated. The model proposed in this study allows to predict the good value of the inertance of the window with a standard deviation under five percent. This model is also used to describe the window impedance of the recorders measured. Since the actual geometry is a rectangular window on a cylindrical tube, the choice between a rectangular (Eq.(16)) or a cylindrical model (Eq.(17)) of right angle bend is not obvious. The two impedances obtained with each of these hypotheses are compared with the measured one for the alto recorder on Fig.3. The cross-sectional area is conserved for the rectangular right angle formulation: $h_p = \pi r_p^2/H$.

The modelled inertances are compared to the estimated inertance from measurements and simulations for the 5 recorders measured in Figure 10. In spite of the poor quality of the measurements, they allow to estimate an inertance near the simulated and the modelled ones for the most of the recorders. For each recorder, both the inertance estimated from the finite element simulation and the one estimated from measurement are much closer to the modelled one with a rectangular right angle bend (Fig.10).

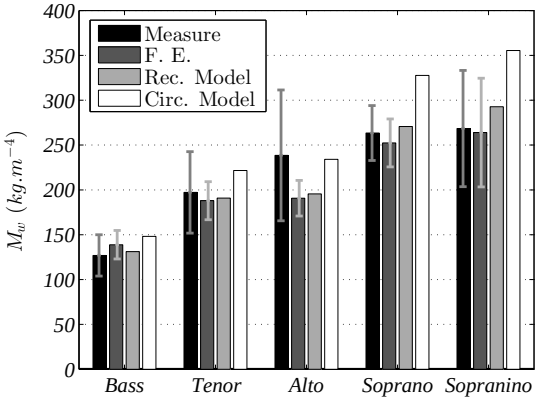

Figure 10: Comparison of the inertances estimated from measurements, from finite element simulations and calculated with the model with a rectangular or circular right angle for the recorders described in tab.1. Error bars indicated the standard deviation of the imaginary part of the impedance measured or simulated from estimated inertances.

5 Discussions

5.1 Comparison with the model of Verge

To understand the comparison between the model of window inertance proposed in this study and the one proposed by Verge [26], it is interesting to rewrite the Verge inertance (Eq.11) as the sum of three inertances as proposed in the equation (18):

$$M_{Verge} = m_{ra}^{(Verge)} + m_{\alpha}^{(Verge)} + \frac{\rho}{WH} l_r^{(Verge)} \tag{24}$$

To do this decomposition it is first interesting to notice that a slit is more or less two successive changes of cross-sections. In the inertance of a right angle bend, the effect of the change of direction is small compared to the effect of the change of cross-section. It appears that the inertance of a rectangular slit is more or less twice that of the inertance of a rectangular right angle bend [10]: $m_{slit} \approx 2m_{ra}^{(rec.)}$. From the equations (11) and (24) the following expressions are therefore obtained:

$$\left\{ \begin{array}{lcl} m_{ra}^{(Verge)} & = & \frac{1}{2} m_{slit} \\ m_{\alpha}^{(Verge)} & = & \frac{1}{2} m_{slit} + \frac{\rho l_e}{S_p} \\ l_r^{(Verge)} & = & \frac{S_w}{S_p} 0.82 r_p = 0.82 r_w \end{array} \right. , \tag{25}$$

where the expression of m_{slit} is given in Eq. (11). With this decomposition the differences between the two models appear clearer. The inertances m_{ra} are similar for the two models.

But the expression chosen in this paper allows taking into account the change of direction in addition to the change of cross-section. The radiation length correction l_r is also similar in the two models. Only the numerical coefficient is different between the two models (see Eq.(18) and Eq.(25)), but the choice of this value is not obvious as discussed in the section 4.1. The major difference is finally located in the inertance m_α related to the angle of the edge. To compare these two models, the ratio of the inertance $m_\alpha^{(Verge)}$ (Eq.(25)) over m_α (Eq.(23)) is studied. The median value of this ratio is around 0.8 if all data are considered (444 geometries). As discussed in section 4, the Verge model is only valid for geometries with sharp edge. The median value of the ratio is around 1 if only these types of geometries are considered (171 geometries, with $\alpha < (\pi/12)$).

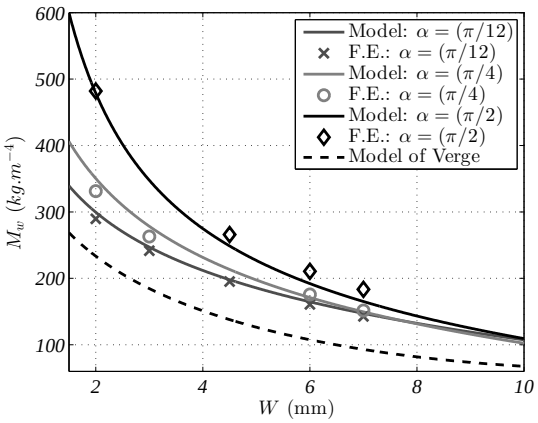

Figure 11: Evolution of the window inertance M_w with the distance W predicted by the new model and the one proposed by Verge (Eq.(11)) for different values of α, other parameters being fixed ($H = 10mm$, $l_e = 5.4mm$, $S_p = 2.4cm^2$). These prediction are comapred to the estimation of the inertance from finite element simulations.

The evolution, predicted by the model of Verge (M_{Verge}, Eq.(11)), of the window inertance with the distance W between the canal and the edge is observed in Fig. 11. It is compared to the evolution predicted by the model proposed in this study and to the inertance estimated from the finite element simulations for different values of edge angle α (see Fig.11). The Verge model underestimates the value of the inertance in addition to not predicting any dependence with the edge angle. The new model appears to improve the prediction and allows predicting the window inertance for a larger set of different geometries than the one proposed by Verge [26].

5.2 Low frequency approximation

The model proposed in this study is based on a simplification using the low frequency approximation of a slightly more complex formula (Eq.(8) and (9)). In these equations the global inertance M_w is split into an inertance m_w and the length l_w of an equivalent straight chimney. By analogy with the study of the side hole impedances, the length l_w could be associated with the height of the ears l_e to which is added the radiation length correction l_r, giving: $l_w = l_e + l_r$. According to this hypothesis, the inertance can be write as $m_w = M_w - \frac{\rho}{S_m}(l_e + l_r)$, which gives:

$$Z_w(\omega) = \frac{\rho c}{\pi r_w^2} \tan\left(jk(l_e + l_r) + \frac{1}{2}(kr_w)^2\right) + j\omega m_w. \tag{26}$$

This formulation, which takes into account the longitudinal resonances in the window, could be used to estimate a more detailed impedance Z_w, which should be valid for a larger range of frequencies. This model predicts a resonance for $kl_w = \pi/2$.

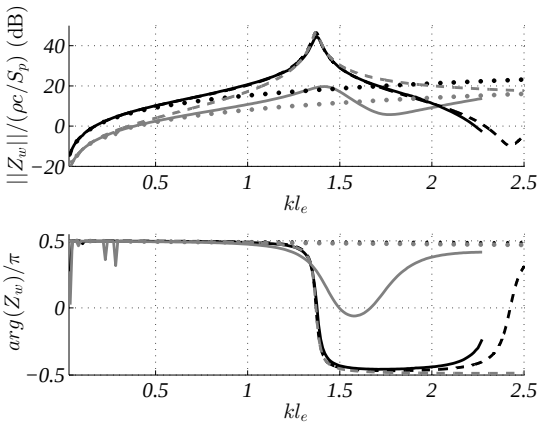

Figure 12: Impedance of windows with high ears ($l_e = 20mm$) for two angles ($\alpha = \pi/2$ (black) and $\alpha = \pi/12$ (grey)), obtained from finite element simulations (solid lines), and calculated with the model without resonance (dots) and with resonance (dash), ($W = 4.5mm$, $H = 12.2mm$ et $S_p = 2.4cm^2$).

For the right angle ($\alpha = \pi/2$), this formula clearly improves the model (black in Fig.12). But for sharper edges (e.g. $\alpha = \pi/12$), the resonance is less marked both for the modulus and the phase (grey in Fig.12). The resonance seems to be followed closely by the antiresonance which decreases the resonance effect for both the modulus and the phase. This effect is not predicted by the formula without the low frequency approximation, which gives a clear resonance (Fig.12). For sharp edges, the low frequency approximation which doesn't give any resonance is a better approximation of the simulated impedance (Fig.12). This specific

resonance is certainly due to the enlargement of the tube during the propagation, like in a conical wave guide. The description existing for the propagation in a conical tube [27], can't be transposed simply to the geometry of the window. Neither the cone with a half-angle $\theta = \pi/4 - \alpha/2$ nor the cone having the same local equivalent radius as the window ($r = \sqrt{WH/\pi}$ at the edge, and $r = \sqrt{H(W + l_e/tan(\alpha))}$ at the top of the ears) give a good approximation of the impedance. It seems that the description of the propagation in the window, which is a rectangular wave guide with an asymmetrical enlargement, is a complex problem which needs a specific study. For classical window geometries, this resonance appears at frequencies out of the range of interest in a musical context (resonance at $f > 10kHz$). For this study the formulation under low frequency is assumed to be enough to describe the radiation. This aspect of the model could be refined further in future.

Another approximation which can be discussed is the assumption that the radius used to calculate the radiation length correction l_r doesn't depend on the angle α. No clear relation is observed between this angle and the residual error of the proposed model compared with the simulations. The assumption that the length l_r depends only of the cross-sectional area $S_w = WH$ seems to be confirmed.

Finally, when modeling the active behavior of the instrument, the position of the sound source among the different aspects described in this study is not well defined. Particularly, if the acoustic source occurs at the extremity of the edge, the inertance related to the right angle m_{ra} should not be included in the window impedance Z_w but in the pipe impedance Z_p (Fig.1,2). For the estimation of the total admittance Y_{to}, it is not really important because the two impedances are added (Eq.(1)). But it can have an importance for a precise estimation of the source term, notably during the attack transient [15].

6 Conclusion

This study proposes a new formulation to model the frequency response of the window of recorder-like instruments. This model is built on equivalent mass approximations and compared with measurements of instruments and with finite element simulations. It explicitly takes into account the presence of the ears and of the edge angle. The frequency response is described through a radiation length l_r (Eq.(18)) and two inertances. The window being a side hole, the change of the acoustic flow direction and the change of the cross-section induce a first inertance which is similar to that of a right angle bend: m_{ra} (Eq.(16) and (17)). The second inertance, m_α given by Eq.(23), is related to the presence of the angle and combines two asymptotic behaviors according the value of the angle of the edge.

This model is compared with a lot of finite element simulations and some measurements. The model presented here is the first to include the angle of the edge. The comparisons with simulations and measurements bring out that the model clearly improves the prediction of the window impedance compared with the few previous models (Fig.11): for the geometry studied here, the standard deviation changes from 22% with the Verge's formulation to 5%.

The model developed in this study neglected the propagation along the chimney defined by the ears and the edge. For classical geometries, the propagation effects should be insignificant in the musical frequency range. However, the inclusion of this propagation is an interesting candidate for improving the model. To model the propagation in this type of duct with a pronounced enlargement would require a specific study. Due to this approximation, the validity domain of the model proposed is limited to low frequencies: $kr_p < 0.5$ and $kl_e < 0.5$, where r_p is the radius of the main tube and l_e the height of the chimney. Due to numerical limitation, the formulation proposed here has only been verified for $f > 100Hz$.

According to the equation (1), the admittance which rules the behavior of the instrument depends on the window impedance and on the body impedance (Eq.(1)). They can finally be written in function of the pulsation ω:

$$\left\{ \begin{array}{rcl} Z_w(\omega) & = & j\omega \left(m_\alpha + \frac{\rho}{S_w} l_r \right) + \frac{\rho}{2\pi c}\omega^2 \\ Z_p(\omega) & = & Z_t + j\omega m_{ra} \end{array} \right. , \tag{27}$$

where ρ is the and S_w is the cross-section of the window. The inertance m_α is associated to the sharpness of the edge can be estimated from the geometry of the window by the equation(23):

$$m_\alpha = \frac{\rho}{H} \tan(\alpha) \ln \left[1 + \frac{l_e}{W \tan(\alpha)} \right] + 32^{-\alpha} \frac{\rho}{H} 0.85 \sqrt{\frac{l_e}{H}} \tag{28}$$

with α the angle in radian of the edge, W the distance between the canal and the edge, H the width of the window and l_e the height of the wall around the window. The inertance m_{ra} is associated to the change of direction of the acoustic flow and depend of the cross-sections of the main tube and the window. In the case of a rectangular window it can be formulated as follow (Eq.(16)):

$$m_{ra} = \frac{2\rho}{\pi H} \left[\ln \left(\frac{1 + \delta^2/4}{2\delta} \right) + \frac{2}{\delta} \left(1 - \frac{\delta^2}{4} \right) \arctan \left(\frac{\delta}{2} \right) \right] \tag{29}$$

where $\delta = 2WH/S_p$ is the ratio of the equivalent cross-section of the window and the main tube (S_p). The length correction linked to the radiation is estimated by the following expression (Eq.(18)):

$$l_r = 0.695 r_w. \tag{30}$$

The impedance Z_t is the input impedance of the tube of the resonator, which can be model by using the formulae summarized by Lefebvre[5]. It is now possible to model the passive frequency response of a recorder-like instrument knowing its geometry.

Acknowledgement

The authors thanks Jean Kergomard for fruitful discussions.

References

[1] B. Fabre and A. Hirschberg, "Physical modeling of flue instruments: a review of lumped models," *Acta Acustica united with Acustica*, vol. 86, no. 4, pp. 599–610, 2000.

[2] R. Auvray, B. Fabre, and P.-Y. Lagrée, "Regime change and oscillation thresholds in recorder-like instruments," *The Journal of the Acoustical Society of America*, vol. 131, pp. 1574–1585, Feb. 2012.

[3] S. Terrien, R. Blandin, C. Vergez, and B. Fabre, "Regime Change Thresholds in Recorder-Like Instruments: Influence of the Mouth Pressure Dynamics," *Acta Acustica united with Acustica*, vol. 101, pp. 300–316, Mar. 2015.

[4] M.-P. Verge, *Aeroacoustics of confined jets : with applications to the physical modeling of recorder-like instruments*. PhD thesis, Technische Universiteit Eindhoven, 1995.

[5] A. Lefebvre, *Computational acoustic methods for the design of woodwind instruments*. PhD thesis, McGill University, 2010.

[6] D. H. Lyons, "Resonance frequencies of the recorder (English flute)," *The Journal of the Acoustical Society of America*, vol. 70, pp. 1239–1247, Nov. 1981.

[7] A. van Steenbergen, "Endcorrections and resonance frequencies of the flue organ-pipe.," Technical Report R-1046-S, University of Technology, Eindhoven, Jan. 1990.

[8] P. Bolton, "www.flute-a-bec.com."

[9] J.-P. Dalmont and J. C. L. Roux, "A new impedance sensor for wind instruments," *The Journal of the Acoustical Society of America*, vol. 123, pp. 3014–3014, May 2008.

[10] A. Chaigne and J. Kergomard, *Acoustics of Musical Instruments*. chap.5.5 (pp.239–243), 7.3 (pp.318–319), 7.6 (pp.360–361), 7.7 (pp.367–372) and 12.6 (pp.686–687), Modern Acoustics and Signal Processing, New York, NY: Springer New York, 2016.

[11] D. H. Keefe, "Acoustical wave propagation in cylindrical ducts: Transmission line parameter approximations for isothermal and nonisothermal boundary conditions," *The Journal of the Acoustical Society of America*, vol. 75, pp. 58–62, Jan. 1984.

[12] F. Blanc, B. Fabre, N. Montgermont, P. De La Cuadra, and A. Almeida, "Scaling of Flute-Like Instruments: An Analysis from the Point Of View of the Hydrodynamic Instability of the Jet," *Acta Acustica united with Acustica*, vol. 96, pp. 642–653, July 2010.

[13] F. Hecht, "New development in freefem++," *Journal of Numerical Mathematics*, vol. 20, Jan. 2012.

[14] R. Auvray, B. Fabre, and P. Y. Lagrée, "Determination of 2d Quasi Incompressible Flow around a Recorder Labium: a Comparison between Different Methods," in *Stockholm Music Acoustics Conference*, (Stockholm, Sweden), 2013.

[15] M. P. Verge, B. Fabre, W. E. A. Mahu, A. Hirschberg, R. R. v. Hassel, A. P. J. Wijnands, J. J. d. Vries, and C. J. Hogendoorn, "Jet formation and jet velocity fluctuations in a flue organ pipe," *The Journal of the Acoustical Society of America*, vol. 95, pp. 1119–1132, Feb. 1994.

[16] V. Dubos, J. Kergomard, A. Khettabi, J.-P. Dalmont, D. H. Keefe, and C. J. Nederveen, "Theory of sound propagation in a duct with a branched tube using modal decomposition," *Acta Acustica united with Acustica*, vol. 85, no. 2, pp. 153–169, 1999.

[17] J.-P. Dalmont, C. J. Nederveen, V. Dubos, S. Ollivier, V. Méserette, and E. te Sligte, "Experimental Determination of the Equivalent Circuit of an Open Side Hole: Linear and Non Linear Behaviour," *Acta Acustica united with Acustica*, vol. 88, pp. 567–575, July 2002.

[18] A. D. Pierce, *Acoustics: an introduction to its physical principles and applications*, vol. 20, chap.7.6 (pp.349–350). McGraw-Hill Book Company, 1981.

[19] P. M. Morse and K. U. Ingard, *Theoretical Acoustics*, chap.9 (p.480–487, p.601–602). Mc graw-Hill book company, 1968.

[20] C. Thompson, "Linear inviscid wave propagation in a waveguide having a single boundary discontinuity: Part II: Application," *The Journal of the Acoustical Society of America*, vol. 75, pp. 356–362, Feb. 1984.

[21] J. C. Bruggeman and T. F. H. v. d. Wetering, "Comment on "Linear inviscid wave propagation in a waveguide having a single boundary discontinuity: Part II: Application" [J. Acoust. Soc. Am. 75, 356–362 (1984)]," *The Journal of the Acoustical Society of America*, vol. 80, pp. 1257–1258, Oct. 1986.

[22] J. C. Bruggeman, "The propagation of low-frequency sound in a two-dimensional duct system with T joints and right angle bends: Theory and experiment," *The Journal of the Acoustical Society of America*, vol. 82, pp. 1045–1051, Sept. 1987.

[23] C. J. Nederveen, "Influence of a toroidal bend on wind instrument tuning," *The Journal of the Acoustical Society of America*, vol. 104, pp. 1616–1626, Sept. 1998.

[24] Keefe, "Theory of the single woodwind tone hole," *The Journal of the Acoustical Society of America*, vol. 72, pp. 676–687, Sept. 1982.

[25] J.-P. Dalmont, C. Nederveen, and N. Joly, "Radiation impedance of tubes with different flanges: numerical and experimental investigations" *Journal of Sound and Vibration*, vol. 244, pp. 505–534, July 2001.

[26] M. P. Verge, R. Caussé, B. Fabre, A. Hirschberg, A. P. J. Wijnands, and A. van Steenbergen, "Jet oscillations and jet drive in recorder-like instruments," *Acta acustica*, vol. 2, no. 5, pp. 403–419, 1994.

[27] A. H. Benade, "Equivalent circuits for conical waveguides," *The Journal of the Acoustical Society of America*, vol. 83, pp. 1764–1769, May 1988.